# Thermal and magnetic properties of chalcogenide CZFTS nanoparticles for solar cell application

E. H. Hussein[a], H. M. Hussein[a], K. A. Mohammed[a,*], R. S. Zbibah[b], A. J. Alrubaie[c], S. Sharifi[d], A. Yazdani[d]
[a]*Department of medical physics, Hilla University College, Babylon, Iraq.*
[b]*Medical Laboratory Technology Department, College of Medical Technology, The Islamic University, Najaf, Iraq*
[c]*Research and Studies Unit, Al-Mustaqbal University College, 51001 Hillah, Babil, Iraq*
[d]*Department of Physics, Tarbiat Modares University, P.O. Box 14115-175, Tehran, Iran*

An attempt is made to resolve the controversy related to the reconstruction mechanism of magneto-optical stannite/kieserite crystal structure with a random mixture of two quaternary compounds of $Cu_2ZnSnS_4$-$Cu_2FeSnS_4$ while the identification of phase formation by XRD is difficult. Since the Fe is surprisingly emerged on the Cu position while Fe is replaced by Zn. The induced dynamical sliding by Cu-ionic-host could be existed which is strongly consequence of magnetic exchange competition (F.M and AFM) through the thermos remanent magnetic reflected on DTA thermal loop. Towards the distortion of intra-plane "a-b", the volume unit cell and c/a are decreased to minimize Gibbs free energy where the band gap energy is also decreased. The broad maximum of Raman spectroscopy is almost decreased linearly. A strong competition between F.M and AF.M due to the distribution of exchange interaction are evident in $x \leq 0.5$ which is dominated by AF.M on x=1.

(Received October 29, 2021; Accepted January 7, 2022)

*Keywords:* Kesterite and Stannite structures, CZFTS nano-crystals, Thermos remanent magnetism, Magnetic exchange interaction, Thin film solar cell, Semiconductors

## 1. Introduction

Although the successful fabrication of the p-type semiconducting quaternary chalcogenide $Cu_2ZnSnS_4$ (CZTS) has been widely presented [1-4], the fundamental optoelectronic characteristic of ground state measurement should be in a challenge. CZTS semiconductor has many similarities between its phases: wurtzite, kesterite and stannite but they have different space groups due to the different distributions of $Cu^{+1}$, $Zn^{+2}$, and $Fe^{+2}$ cations [4]. CFTS has a stannite structure with cubic (P-43m, a=5.42 ˚A), tetragonal (I-42m, a=5.45 Å, c=10.76 Å), and wurtzite (P-4, a=5.43 Å, c=5.41 Å) phases with a direct band gap of 1.2–1.5 eV [5]. CZTS is typically shown in a kesterite structure with tetragonal and wurtzite phases with a direct band gap in the range 1.4–1.6 eV [6, 7]. The cause of the broad variety of lattice parameter in each composition (CZTS kesterite [8-12] and CFTS stannite [4, 8, 9, 13, 14]), could be an effective parameter on the variation of optical property (due to band gap), which has not been clarified yet [4, 11, 14-20]. It is evident that the band gap variation of CZTS is reasonably higher than that of CFTS resulting in the bandwidth of Fe reflected on its higher electronegativity compared to $Zn^{+2}$ [4] and magnetic exchange energy [20], but the mechanism is not clarified. Shibuya and co-workers [21] investigated theoretically the influence of the incorporation of Fe/Zn on the structural transition from kesterite to stannite. They have also investigated the lattice constants, band gap, and enthalpy for CZTFS alloys and confirmed a phase transition from kesterite (Zn-rich) to stannite (Fe-rich) at (Fe/ Zn) ~0.4.

* Corresponding author: kahtan444@gmail.com
https://doi.org/10.15251/CL.2022.191.9

However, they stated that the alloy compositions of CZTS based on Fe could be used in Si tandem solar cells. Huang et al [22] have synthesized CZFTS via a hot injection method by varying x=Fe / (Zn + Fe). They reported the structural transition from stannite to kesterite at x=0.4 for CZTFS. They have also reported the potential improvement of photoelectrical conversion performance by partially substituting Zn with Fe in $Cu_2ZnSnS_4$. Due to difficulty in identification of the structural phase for stannite and kesterite because of the similarity in their space groups, all efforts made to overcome the difficulty in controlling secondary phases [23], grain growth [24-26], band gap gradient [27], defect formation, and the variety range of crystalline structure [5-12]. It seems that strong bond rupturing of atomic displacement through replacing $Fe^{+2}$ with $Cu^{+1}$ can help us to clarify identification of the structural phase for stannite and kesterite. Since the results are strongly sensitive to the synthesis method and experimental bath environment (chemical reaction), the following parameters should effectively control the synthesis reaction:

(i) Thermal activation of chemical reaction at the interface of contribution compositions.

(ii) The different strength of chemical potential in the Gibbs free energy, by which the $G = U - TS$ should be replaced by $F = U - TS + \sum \mu_i dN_i$,

(iii) The difference between electronegativity's of Zn=1.65 and Fe=1.89 where it is surprisingly evidence that the Fe is appeared to site on Cu-position while it is replaced by Zn.

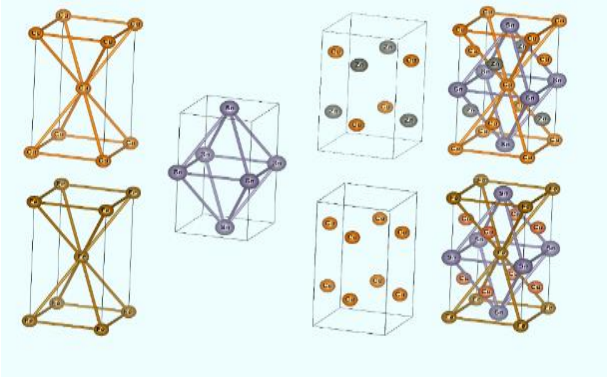

*Fig. 1. Crystal structure of $Cu_2ZnSnS_4$ and $Cu_2FeSnS_4$ to represent the Cu-host in order to rearrange the different positions of Zn and Fe, despite the replacement of Fe on Zn.*

Although, the magnetic exchange energy [25] with focusing on the optical properties [28-30] is studying on wide range of research, the interface chemical potential of the two random mixed quaternary compounds should be in challenge [5]. The effect is strongly evidence in:

(a) The changeable atomic positions of "Cu-Zn-Fe" in the crystal structural formation (Figure 1).

(b) The variation of the lattice constants, unit cell volumes and band gap energy $E_g$. where the strength of variation range could be consequence of the s-d hybridization strength of Fe. Whereas the duality of the electron could result on the competition of redistribution of magnetic exchange which could be affected by s-p character (Figure 2).

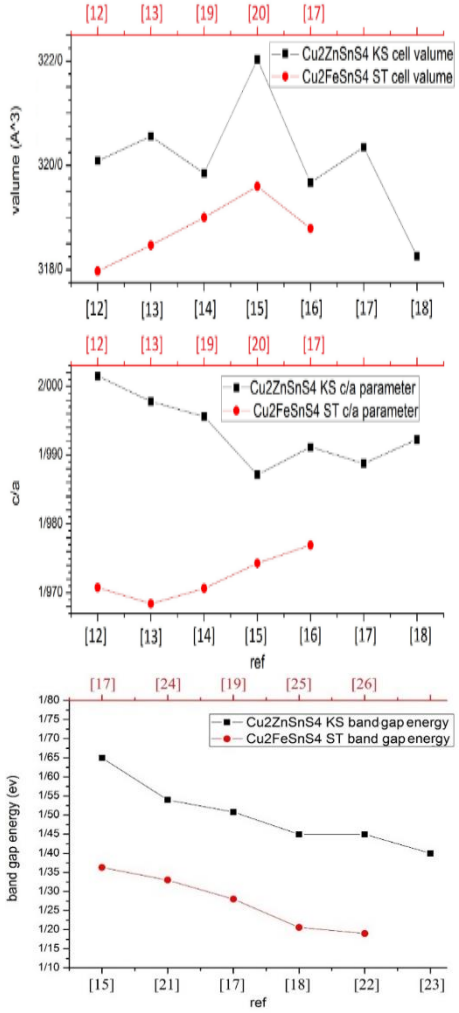


*Fig. 2. Variation of volume, c/a and bandgap extracted from references specified in the figure for different crystal structures of kesterite $Cu_2ZnSnS_4$ and stannite $Cu_2FeSnS_4$.*

It seems that the formation of the first transition phase due to the bond-rupturing atomic displacement should be the cause of the effect. However, the strong cation-anion formation could be directed towards the lower energy of the crystal structure formation. Where the atomic position of $Cu^{+1}$ band offset of the interface can control the location of Zn/Fe [4,6] and the effect of dynamic character of substitution of $Fe^{+2}$ by $Zn^{+2}$ should be the onset of magnetic coupling exchange in optical character of crystal structure. The control could be by varying lattice constant and varying absorption range of Raman and UV-Vis spectra. Whereas the band gap gradient may be one crucial factor for optimizing the kesterite /stannite-bases solar cells, since the different variable ranges of band gap in each side (CZTS)-(CFTS) could be an effective parameter in order to understand the topological atomic positions, which are more evident in "CZFSNS". However, following our previous work [19] here the dynamical atomic displacement related to the topological atomic positions, reflect on the tuning of experimental environment (bath) of thermochemical reaction which is controlled by the solvothermal synthesis method by varying x is investigated. This could be strongly evident that the bond rupturing atomic displacement is due to the induced thermos remanent magnet. It could be a consequence of competition between F.M and AF.M exchange interaction reflected on decreased lattice constant, band gap energy wide plateau UV vis and broad peak of Raman shifts to lower frequencies in direction to stabilize the stannite structure.

## 2. Materials and methods

Since the stable phase formation is a consequence of minimum Gibbs free energy (F= U-TS+$\sum \mu_i dN_i$) due to the molecular dynamics and thermal activation by coupling to an external-chemical-reaction bath at a constant temperature (and/or pressure), it could be replaced with an adjustable time constant. Thus, it is supposed that the solvothermal synthesis could be a suitable method. However, the phase formation of "$Cu_2ZnSnS_4$-$Cu_2FeSnS_4$" is formed at the interfaces of three binary components of the metallic-sulfide $Cu_2S$–ZnS-$SnS_2$ where $FeS_2$ is reported to be formed instead of FeS in thermodynamically heat-exchange bath. The difficulties in the phase formation of each binary of intermetallic sulfide is more evident in the phase diagram [23], whereas the phase formation of "Sn-S" is easier than the others (i.e. 3d-metallic Cu-S and Zn-S by the only one composite of α, β ZnS formation [23]). In this regard, 2 mmol copper(II) chloride ($CuCl_2$; Merck,), (1-x) mmol zinc chloride ($ZnCl_2$; Merck), x mmol iron(II) chloride tetrahydrate ($FeCl_2{\cdot}4H_2O$; Merck), where x is 0 (Fe-0), 0.1 (Fe-0.1), 0.5 (Fe-0.5), 0.9 (Fe-0.9), 1 (Fe-1), 1 mmol tin(II) chloride dihydrate ($SnCl_2{\cdot}2H_2O$; Merck), 4 mmol Thiourea (TU) ($CSN_2H_4$; Merck, 99.9%), 0.64 g Polyvinylpyrrolidone (PVP; Merck) as capping agent and 40 ml ethylene glycol (EG; Merck) as solvent were mixed and then stirred uniformly and then it was heated at 80 °C for 30 min. The resulting suspension was transferred into the Teflon container of an autoclave with a volume of 50 ml and held at 220 °C for 24 hours. The resulting suspension was washed with ethanol and DI water for three times by centrifuging with the rate of 9000 rpm. Finally, the sediment was dried in vacuum at 100 °C for 2 hours. Structural properties and phase identification of the samples were examined by X-ray diffraction (XRD) patterns using a diffractometer system (D8 Advance Bruker) supplied by a Cu-Kα λ=1.54 Å radiation source and high-resolution Raman spectroscopy (SENTERRA, laser wavelength λ=785 nm, Spectral Resolution: < 3 $cm^{-1}$). The optical properties of the films were determined by a Shimadzu UV-1800 and finally the magnetization was measured on the static magnetic field 0-15 Os at room temperature.

## 3. Results and discussion

Since the formation of cation-anion could be a consequence of the chemical activation of the interface, the reduction of Zn+2/Cu+1/ Fe+2(+1) charge redistribution in "a" direction to a lower energy of the crystal structure seems to be the main cause where the DTA thermal loop could be consequent of the commensurate of the induced thermos remanent magnetic mechanism figure 3. The DTA is measured for X>0.5 around which the competition of magnetic exchange distribution is dominated and below which the wide ranges unstable variation of unit cell volume and band gap energy are more pronounced in figure 2 in Zn rich side while the variation value of stannite (Fe-rich) is lower and more stable than the Kesterite (Zn-rich). Since the equilibrium minimized crystal energy is a consequence of simultaneously minimization of the unit cell volume and c/a, the band offset of the structure, the variation of experimental results is strongly considered to be a dynamical character consequence of: The sliding of atomic positions of Fe/Zn/Cu1+ resulting in the charge distribution to minimize structure energy of Fe site appear to be at Cu position due to modulation of strength of S-d hybridization resulted on the induced thermos remanent magnetic character by which the competition of F.M and AF.M could be the cause of magnetic exchange distribution as shown in figure 4. The effects are also more pronounced on the small spread maximum peaks of X ray on Zn reach side figure 5. Since the crystalline phase structures are commonly similar in X-ray diffraction patterns which is shown in figure 5 (an emerging peak at (105) and shouldering formation before (112) on the Fe-rich side), only the stability of minimum energy formation should be different. Although, the maximum peaks in Fe-rich side are sharper while it is spread in Zn rich side. The cause is supposed to be due to the bond rupturing atomic displacement related to the different chemical activation potentials due to induced thermos remanent magnetic character, which strongly affect the first transition phase formation [31]. It is shown in figure 1, although "Fe" is replaced by "Zn", but the "Fe" is placed on "Cu" site, resulting in the more stability of crystalline structure. The cause of the more stability can be due to the magnetic exchange energy (antiferromagnetic order) for x=0.9 and 1 figure .4,

which can be the cause of the decreased volume of unit cell resulting in the band gap energy (Figure 5). However, although the displacement of atomic positions is more obvious in the opto-magnetic crystalline structure, but regarding the binary phase formation in the phase diagram [32] resulting in three contributions of opto-electronic structure of ZnS, $Cu_2S$ and $SnS_2$ ( where $FeS_2$ is reported instead of FeS )is in direction to the stable quaternary phase formation. It could be a question whether; (1) the balancing of the contribution of cation-anion-distributions of $Cu^{+1}$, $Zn^{+2}$ and $Sn^{+4}$ related to the sulfur precursor "$S^{-2}$" or (2) the competition of at least two-different (covalent + ionic) chemical bonds. Whereas both are related to the high tolerance of stoichiometric variation and the tunable Fermi energy level could be the cause of the band offset each of which are because of different chemical reaction due to three ternary compound of the minimization of Gibbs free energy "G=U-TS" replaced by the relation of $G = U - TS + \sum \mu_i N_i$ . While firstly the lowering entropy due to emergence of magnetic exchange ordering should be compensated. Secondly the reduction of valence electron band on dynamical sliding of $Fe^{2+}$ to site at $Cu^{1+}$ position through the $Zn^{2+}$ should be compensated. However, the interface chemical potential could be the cause of bond rupturing of atomic displacement to achieve the equilibrium band offset [31]. Whereas, in our solvothermal synthesis method, the chemical reaction bath was at about 200 and 280℃ in a high boiling point organic solvent oleylamine (OLA) or octadeceen (ODE) in order to archive high-quality quaternary nanocrystalline [17-19].

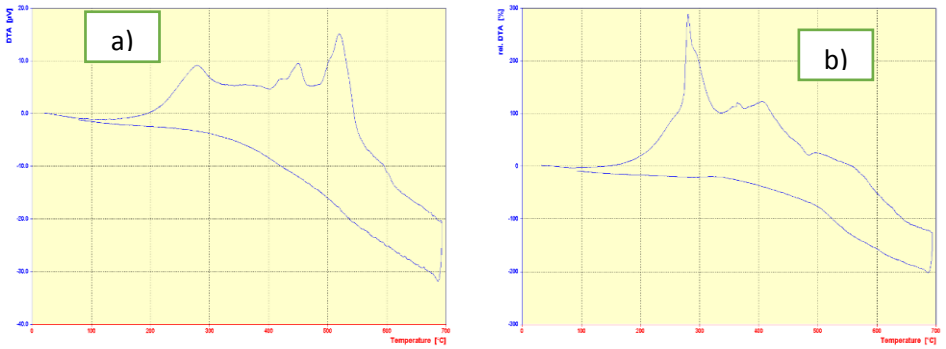


*Fig. 3. DTA thermal loop curve for different Fe concentration a) Fe 0.5 b) Fe 1.*

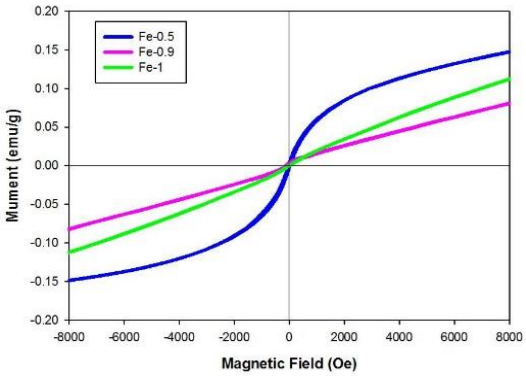


*Fig. 4. Variation of VSM curves for various Fe/Zn ratios in CZFTS.*

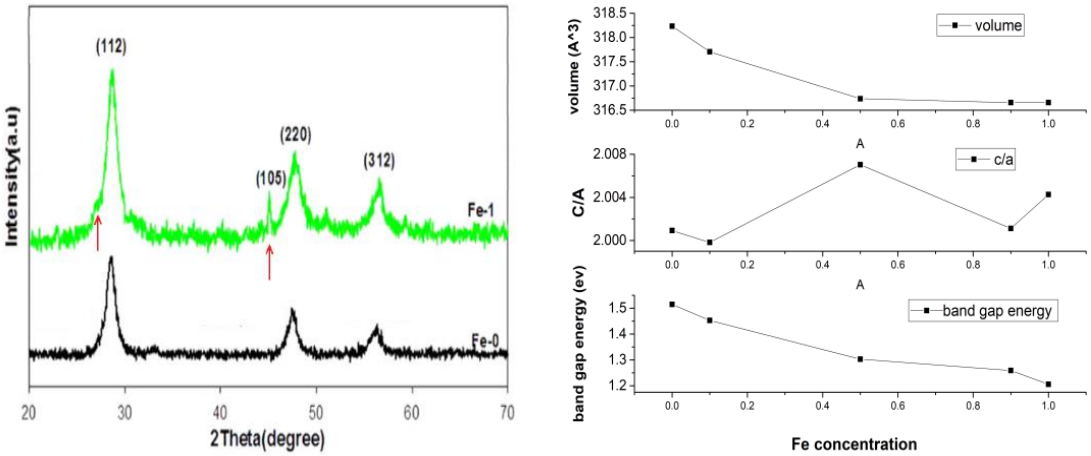


*Fig. 5. XRD pattern for x=0 and 1 and Variation of volume, c/a and band gap energy versus the replacement of Fe on Zn.*

Consequently, although the thermodynamical stabilities of four CZTS structures by first principles calculation are reported to be in the order of kesterite >stannite>WZ-kesterite >WZ-stannite, but here because of mentioned intrinsic character of substitution of $Fe^{2+}$ at $Cu^{1+}$ through $Zn^{2+}$:

(i) the requirement chemical potential for the minimization of Gibbs free energy and the bond rupturing of topological atomic displacement closely related to the mechanism of dynamical sliding in the stable crystal phase formation and

(ii) The induced magnetic exchange energy, the $Cu_2FeSnS_4$ stannite, is shown to be more stable than kesterite , which is more evident in experimental results.

Consequently, the structural behavior of $Cu_2(Zn,Fe)SnS_4$ compositions is investigated on the following observation which has strongly showed a dependence of crystal-structure on the magnetic-ions, which is strongly evidence of Raman spectroscopy (Figure 6).

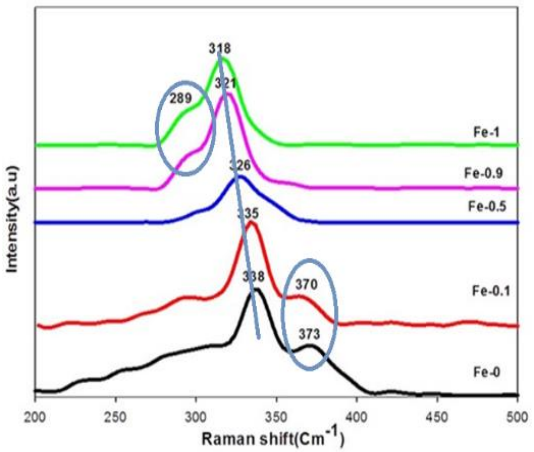


*Fig. 6. Variation of Raman spectroscopy measurement for various Fe/Zn ratio 0<x≤1 in CZFTS.*

Figure 5 shows the variation of room temperature XRD studies of the lattice parameter with x resulted to a nonlinear dependence on substitution of $Fe^{+2}$. A strong positive deviation from Vegard's rule (especially x≤ 0.5) which is one of the most frequency used methods to detect an unstable magnetic structure is more evidence. It is evidence that the both "volume" and $\frac{c}{a}$

drastically decreasingly depend on the "x" and become more unstable in the range of "0.4-0.6". The variation is more prominent at x≅ 0.5, where the main magnetic instability occurs, and we may assume a distribution of magnetic-exchange in addition to dynamic sliding of atomic displacement. The effects are naturally due to the competition of CFE and exchange-interaction in direction to probably spread of maximum of Raman at x=0.5 (Figure 6) at which a symmetrical small shouldering effect (transfer from right to the left of maximum) of lowering of the cohesive energy is observable. This effect is more evidence on decreasing C-lattice constant interlayer, in spite of intra-layer variation of a lattice constant direction. The distortion effects could be due to the stretching of X ray-plane where the magnetic-$Fe^{+2}$-ion is located at the center and at the corner $(8\times\frac{1}{8})$ of unit cell, magnetically resulting in the decreased c-direction. The proposed intrinsic structural effects due to the position of Fe strongly affect the band-gap energy in direction to the decreasing non-linear function. Consequently, the simultaneous decreasing of $\frac{c}{a}$ and volume of unit cell $\Delta V = V_{Ks} - V_{St}$ could be due to the compressing of the c-direction resulting in the stretching of "x-y" intra-layer where the decreased band gap $\Delta E = E_{Ks} - E_{St}$ could be due to the crystal field effect of "JT" distortion resulted from the completion of DTA thermal loop figure.3 and moderation of induced magnetic field by $Fe^{+2}$ substructure. Regarding the "JT" structural distortion due to the magnetic exchange energy resulting in the lower minimum Gibbs free-energy, it could arise a question, whether the effects are consequences of the topological structural distortion resulted from the different positions of $Cu^{+1}$, $Zn^{+2}$, $Fe^{+2}$, $Sn^{+4}$ and/or they are due to the competition strength of the "cation-anion" chemical bond formation, or even both of the super/double-exchange and the exchange interaction between $Fe^{+2}$-$Fe^{+2}$. To clarify the effects, both Raman and UV-Visible spectra in addition to differential thermal analysis and magnetization measurement were investigated. It is while (i) the variation of lower symmetry crystal structure, the strength of chemical bond that is sensitive to local atomic-environment, could be described by the related experimental results (ii) the thermos-chemical activation owing to the interface chemical potential is resulted to thermal DTA loop (figure 3).The variation of Raman spectra related to the substitution of $Zn^{+2}$ by $Fe^{+2}$ is shown in figure 6 It is evident that in addition to the variation range of main peaks located at 318 (A1) and 289 (A1) $cm^{-1}$ for x=1, and 338 (A) $cm^{-1}$ for x=0, which linearly shifts toward the lower wavelengths, some shouldering effect is also observed symmetrically around the maximum before (right at 373 $cm^{-1}$ for x=0) and after (left at 289 $cm^{-1}$ for x=1). To compare with previous reports, A1 and A, symmetry modes for stannite and kesterite structures are related to pure sulfur anion vibrations, respectively, where these modes dependent on the Fe–S and Zn–S bonding [11]. It is also obvious that while FWHM at x=0.5 is wider than the other cases, the shouldering effect is vanished resulting in the distribution of main maximum. The effects supposed to be due to critical fluctuation of phase transition resulting in both band offset of bond-rupturing atomic displacement and anisotropy exchange due to distribution of exchange interaction at x=0.5.

Regarding to the shouldering effect, it is more pronounced that while it is distributed strongly before and weakly after the main maximum in the Zn-rich side, it appears to be only after the main max in the $Fe^{+2}$-rich side.

The effect of such shouldering effect around the main maximum is strongly meaningful defining the stable formation of Gibbs free energy resulting in the lower symmetry due to "JT" distortion effect.

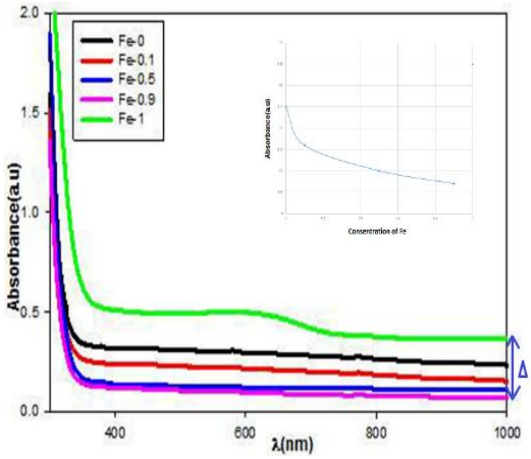


*Fig. 7. The effect of variation of Fe/Zn ratio (0<x≤1) in CZFTS in UV-visible absorption spectra, where the trend shows as Fe increases, and the absorption intensity.*

This shift toward the lower-energy could be consequence of the attraction magnetic dipole energy resulted to decrease of $\frac{c}{a}$ and unit cell volume in direction to stabilize structure. The effect is supported by the UV-visible absorption, on the construction region of wavelength in the range of 380-1000 nm" (Figure 7), where there is no evidence for optical absorption intensity while a small decrease on absorption value is more evidence as the substituted amount of $Fe^{+2}$ increases .The both decrease of $E_g$ and plateau unchanged in the wavelength range of 380-1000nm is supposed by the consequence of thermal lattice vibration due to thermos remanent magnetic exchange resulted to completion and redistribution of F.M and AF.M exchange energy which is more evidence at x=0.5 fig.4. The effect could change the stability of crystal structure through the minimum Gibbs free energy because of entropy variation dS=dQ/T where the band offset reaches its equilibrium. From all descriptions of the optical character of crystal structure measurements on the suggested less symmetrical minimum Gibbs free energy in the Fe-rich-side. It can be concluded that the magnetic exchange energy could be the main cause of the lower-energy structure resulted from the position of $Fe^{2+}$.

To clear out the effects and the investigated assumption, the DC-VSM at room temperature was performed on the static strength of magnetic field 0-1.5 kOe at room temperature and are shown in Figure 4.

It is strongly evident that the magnetic exchange interaction is characterized completely by the super-paramagnetism state in Fe-rich side (x=0.9 and 1), in direction to compress the unit cell in relation to the position of $Fe^{+2}$, where both $\frac{c}{a}$ and volume of unit cell are decreased (Figure 6). Although the opto-crystalline structure is supposed to be on its more stable form, but in order to evaluate the bond rupturing of atomic displacement, the DTA thermal loop was considered. It is strongly evidence that in addition to the existence of thermal loop energy on x=0.5 which is stronger than x=1 some soft peak distributions as possibility of displace atomic position without any crystalline phase transition due to thermos-chemical activation should be emerged. Although the opto-magneto-crystallinity of the system $x \geq 0.6$ should be conditionally stable as ferromagnetic, but the magnetic structure is the unstable magnetic character, where the surprisingly weakly ferromagnetic or competition between FM and super para magnetism due to the distribution of exchange are clearly obvious in the Zn-rich-side x= 0.1, 0.5. The magnetic exchange fluctuation resulting from the spatial distribution of magnetic ions is more evident in the experimental results of Raman spectra (Figure 6).

## 4. Conclusion

According to the all following results, it could be suggested that the Fe/stannite structure should be more stable than the Zn/kieserite, due to both magnetic exchange energy and JT distortion effect on dynamical creep of substitution of $Fe^{+2}$ on $Zn^{+2}$.

The decreased volume of unite cell and $\frac{c}{a}$ on which the decrease of c-direction could effectively stretch the intra layer of X-Y-direction.

The lower UV-Vis absorption in the wavelength range of 380-1000 nm in the region of $0.1<X<0.9$ resulted to the almost linearly band-gap decrease.

The linear decrease of the maximum region in Raman spectrum with some shouldering effect around the maximum could be strongly due to the redistribution of symmetry of the crystal structure resulting in the charges of constituent element. The effect could also result from the dynamical bond-rupturing atomic displacement in direction to minimum Gibbs free energy resulting from "JT" distortion. The proposed suggestion is strongly evident in the magnetization measurements, whereas the structure is super para magnetism.

Therefore, the magnetization measurements strongly depend on the Fe concentration in the two different ranges of $0<x\leq0.5$ and $1\leq x<0.5$.

Since the magnetic structure is traditionally a consequence of the composition exchange and anisotropy, here the effects are controlled by the topological metallic positions resulting in both metal distribution and inter-metallic dislocation by thermo-magnetic remanent reflected on DTA thermal loop energy.

Consequently, because of the band offset of different topological atomic positions of Fe and Zn, which should affect the displacing atomic sliding resulted to the thermos-chemical activation and the distribution of exchange interaction, the magnetization measurement is considered on two different ranges of concentration, i.e. $0\leq x\leq0.5$ for diluted Zn-side (Figure 9) and $1\leq x<0.5$ for $Fe^{+2}$ rich side.

In the Fe-rich side, the position is almost fixed and the exchange interaction dominates. Whereas, the magnetic structure is expected to be super para magnetism as it is shown in Figure 8, but at the lower concentration, $0<x\leq0.5$, the anisotropy exchange dominates and the competition between ferromagnetism through thermo-magnetic activation and "superparamagnetism" due to exchange distribution play a big role resulting in the unstable low magneto-crystalline structure.

## References

[1] A. Tombak, Y. Selim Ocak, M. Fatih Genise, T. Kilicoglu, Materials Science in Semiconductor Processing 28, 98 (2014); https://doi.org/10.1016/j.mssp.2014.07.006

[2] Sh. C. Riha, B. A. Parkinson, A. L. Prieto, Journal of the American Chemical Society 131, 12054 (2009); https://doi.org/10.1021/ja9044168

[3] Z. F. Sonnenenergie, W. F. Baden-Wurttemberg, ZSW produces a thin-film solar cell with 20.3 percent efficiency, Press release 08/2010, (2010) Stuttgart, Germany.

[4] P. A. Fernandes, P. M. P. Salome, A. F. da Cunha, Journal of Alloys and Compounds 509, 7600 (2011); https://doi.org/10.1016/j.jallcom.2011.04.097

[4] D. B. Khadka, J. Kim, Journal of Physical Chemistry C 118(26), 14227 (2014); https://doi.org/10.1021/jp503678h

[5] Z. Xiaoyan, N. Bao, K. Ramasamy, B. Lin, A. Gupta, Photovoltaic Specialists Conf. (PVSC), 38th IEEE, 001967 (2009).

[6] Y. Li Zhou, W. Hui Zhou, M. I. Li, Y. Du Fang, S. Wu Xin, Journal of Physical Chemistry C 115, 19632 (2011); https://doi.org/10.1021/jp206728b

[7] X. Lu, Z. Zhuang, Q. Peng, Y. Li, Chemical Communications 47, 3141 (2011); https://doi.org/10.1039/c0cc05064d

[8] S. Schorr, H. J. Hoebler, M. A. Tovar, European Journal of Mineralogy 19, 65 (2007);

https://doi.org/10.1127/0935-1221/2007/0019-0065
[9] P. Bonazzi, L. Bindi, G. P. Bernardini, S. A Menhetti, Canadian Mineralogist 41, 639 (2003); https://doi.org/10.2113/gscanmin.41.3.639
[10] T. K. Todorov, K. B. Reuter, D. B. Mitzi, Advanced Materials 22, (E1562010).
[11] Y. Zhang, X. Sun, P. Zhzng, X. Yuan, F. Huang, W. Zhang, Journal of Applied Physics 111, 063709 (2012); https://doi.org/10.1063/1.3696964
[12] M. Himmrich, H. Haeuseler, Spectrochim Acta 47A, 933 (1991); https://doi.org/10.1016/0584-8539(91)80283-O
[13] X. Jiang, W. Xu, R. Tan, W. Song, Chen, Materials Letters 102-103, 39 (2013); https://doi.org/10.1016/j.matlet.2013.03.102
[14] S. R. Hall, J. T. Szymanski, J. M. Stewart, Canadian Mineralogist 16, 131 (1978).
[15] Q. Luo, Y. Zeng, L. Chen, C. Ma, Chemistry-An Asian Journal 9(8), 2309 (2014); https://doi.org/10.1002/asia.201402152
[16] Bulletin of advanced technology research 5(8), 51 (2011).
[17] Z. Shadrokh, H. Eshghi, A. Yazdani. Materials Science in Semiconductor Processing 40, 752 (2015); https://doi.org/10.1016/j.mssp.2015.06.082
[18] M. Cao, C. Li, B. Zhang, J. Huang, L. Wang, Y. Shen, Journal of Alloys and Compounds 622, 695 (2015); https://doi.org/10.1016/j.jallcom.2014.10.164
[19] Z. Shadrokh, A. Yazdani, H. Eshghi, Semiconductor Science and Technology 31, 045004 (2016); https://doi.org/10.1088/0268-1242/31/4/045004
[20] Y. Cui, R. Deng, G. Wang, D. A. Pan, Journal of Materials Chemistry 22, 23136 (2012); https://doi.org/10.1039/c2jm33574c
[21] T. Shibuy, Y. Goto, Y. Kamihara, M. Matoba, K. Yasuoka, L. A. Burton, A. Walsh, Applied Physics Letters 104, 021912 (2014); https://doi.org/10.1063/1.4862030
[22] C. Huang, Y. Chan, F. Liu, D. Tang, J. Yang, Y. Lai, J. Li, Y. Liu, Journal of Materials Chemistry A 1, 5402 (2013); https://doi.org/10.1039/c3ta00191a
[23] Desk Handbook: Phase Diagrams for Binary Alloys, Hiroaki Okamoto, ISBN: 0-87170-682-2, ASM International ® Materials Park, OH 44073-0002
[24] A. Carrete, A.Shavel, X. Fontane, J. Montserrat, J. Fan, M. Ibanez, E. Saucedo, A. Perez-Rodriguez, A. Cabot, Journal of the American Chemical Society 135, 15982 (2013); https://doi.org/10.1021/ja4068639
[25] S. Suehiro, K. Horita, K. Kumamoto, M. Yuasa, T. Tanaka, K. Fujita, K. Shimanoe, T. Kida, The Journal of Physical Chemistry C 118, 804 (2014); https://doi.org/10.1021/jp408360j
[26] M. J. Thompson, T. P. A. Ruberu, K. J. Blakeney, K. V. Torres, P. S. Dilsaver, J. Axial Vela, The Journal of Physical Chemistry Letters 4, 3918 (2013); https://doi.org/10.1021/jz402048p
[27] C. Tablero, Journal of Physical Chemistry C 116, 23224 (2012); https://doi.org/10.1021/jp306283v
[28] A. Singh, H. Geaney, F. Laffir, K. M. Ryan, Journal of the American Chemical Society 134, 2910 (2012); https://doi.org/10.1021/ja2112146
[29] X. L. Liang, P. Guo, G. Wang, R. P. Deng, D. C. Pan, X. H. Wei, RSC Advances 2, 5044 (2012); https://doi.org/10.1039/c2ra20198d
[30] A. Gillorin, A. Balocchi, X. Marie, P. Dufour, J. Y. Chane-Ching, Journal of Materials Chemistry 21, 5615 (2011); https://doi.org/10.1039/c0jm03964k
[31] V. P. Dmitriev, S. B. Roschal, Yu. M. Gufan, P. Toledano, Physical Review Letter 60, 1958 (1988); https://doi.org/10.1103/PhysRevLett.60.1958
[32] A. Yazdani, Z. Shadrokh, H. Eshghi, Material Research Bulletin 80, 159 (2016); https://doi.org/10.1016/j.materresbull.2016.03.036